

# Rheology of Passive and Adhesion-Activated Neutrophils Probed by Atomic Force Microscopy

Pere Roca-Cusachs, Isaac Almendros, Raimon Sunyer, Núria Gavara, Ramon Farré, and Daniel Navajas

Unitat de Biofísica i Bioenginyeria, Facultat de Medicina, Universitat de Barcelona–IDIBAPS, 08036 Barcelona, Spain

**ABSTRACT** The rheology of neutrophils in their passive and activated states plays a key role in determining their function in response to inflammatory stimuli. Atomic force microscopy was used to study neutrophil rheology by measuring the complex shear modulus  $G^*(\omega)$  of passive nonadhered rat neutrophils on poly(HEMA) and neutrophils activated through adhesion to glass.  $G^*(\omega)$  was measured over three frequency decades (0.1–102.4 Hz) by indenting the cells 500 nm with a spherical tip and then applying a 50-nm amplitude multi-frequency signal.  $G^*(\omega)$  of both passive and adhered neutrophils increased as a power law with frequency, with a coupling between elastic ( $G'$ ) and loss ( $G''$ ) moduli. For passive neutrophils at 1.6 Hz,  $G' = 380 \pm 121$  Pa, whereas  $G''$  was fourfold smaller and the power law coefficient was of  $x = 1.184$ . Adhered neutrophils were over twofold stiffer with a lower slope ( $x = 1.148$ ). This behavior was adequately described by the power law structural damping model but not by liquid droplet and Kelvin models. The increase in stiffness with frequency may modulate neutrophil transit, arrest, and transmigration in vascular microcirculation.

## INTRODUCTION

The mechanical properties of leukocytes, and neutrophils in particular, and the changes they suffer during activation play a key role in determining their function in response to inflammatory stimuli (1,2). Pulmonary microcapillaries, with diameters that can be smaller than those of neutrophils (3), induce retention of neutrophils (4). This retention, which increases the probability of transendothelial migration (1), is probably due to the process of deformation that neutrophils undergo when entering microcapillaries, which is dependent on neutrophil mechanical properties. Indeed, the retention of neutrophils in microcapillaries is known to increase with neutrophil stiffness (4). Additionally, the stiffness of leukocytes could also regulate their adhesion to the endothelium in larger blood vessels by modulating the contact area between leukocytes and the endothelium (5–7). Neutrophil deformation and recovery during microvascular transit are dynamic processes involving a wide range of timescales. Therefore, apart from a characterization of stiffness, knowledge of neutrophil rheology as a function of activation and for a broad range of frequencies or timescales is necessary to better understand the pathophysiological implications of neutrophil mechanics. However, existing techniques measuring neutrophil rheology present limitations in controlling the activation state of neutrophils, in unambiguously determining their complex shear modulus  $G^*(\omega)$ , or in providing measurements at a range of frequencies wide enough for an adequate characterization.  $G^*(\omega)$  defines the mechanical constitutive equation of the cell and provides knowledge of the cell stress-strain response in a model-independent manner. The limitations of

existing techniques have led to contradictory descriptions of the rheology of passive neutrophils and its changes with activation.

Leukocyte rheology has been studied extensively through the micropipette aspiration technique (8–11). This technique consists generally in the aspiration of a leukocyte with a micropipette having a diameter smaller than that of the leukocyte, which causes the cell to extend a protrusion into the micropipette. The evolution of this protrusion is then recorded through the acquisition of optical microscopy images as a function of time, aspiration pressure, and micropipette radius. The observed resistance of leukocyte protrusions to enter micropipettes and the subsequent resistance to flow were interpreted through different viscoelastic mechanical models. These models, which were characterized by one or two time constants, described leukocytes as either an elastic cortex enclosing a Newtonian (8,9,12) or Maxwell (10,13) liquid or as standard viscoelastic (Kelvin) bodies (11,14). However, micropipette aspiration experiments present several limitations. First, the high levels of deformation involved might alter the state of the leukocyte. Indeed, leukocytes have been observed to activate and modify their mechanical properties when forced to enter narrow channels (15). Second, the considerable deformation and the complicated contact geometry present in experiments require complex calculations to obtain leukocyte mechanical parameters. This results in calculated mechanical parameters which generally depend on the assumed leukocyte mechanical model and do not provide a direct estimation of  $G^*(\omega)$ . Finally, the range of timescales or frequencies observable in micropipette aspiration tests is reduced due to the limitations given by image acquisition rate (high frequency limitation) and by the time it takes for leukocyte protrusions to extend fully (low frequency limitation).

Submitted May 12, 2006, and accepted for publication July 20, 2006.

Address reprint requests to Daniel Navajas, PhD, Professor of Physiology, Unitat de Biofísica i Bioenginyeria Facultat de Medicina–Universitat de Barcelona Casanova, 143 08036-Barcelona, Spain. Tel.: 34-93-402-4515; Fax: 34-93-402-4516; E-mail: dnavajas@ub.edu.

© 2006 by the Biophysical Society

0006-3495/06/11/3508/11 \$2.00

doi: 10.1529/biophysj.106.088831

The limitation in frequency range has been overcome by rheological measurements on neutrophils made with magnetic twisting cytometry (MTC), a technique which probes cell mechanical properties by binding magnetic microbeads ( $\sim 5 \mu\text{m}$  in diameter) to the cell membrane with specific cytoskeletal receptors, oscillating the beads horizontally with an external magnetic field, and measuring the resulting bead displacement. By calculating an apparent complex modulus  $g^*(\omega)$  (defined as the ratio between applied torque and bead displacement) over four frequency decades (0.1–1000 Hz) with MTC, Fabry et al. (16) observed a scale-free behavior with frequency. These results were analyzed with a power law structural damping model and interpreted through soft glassy rheology (SGR) (17). SGR explains this behavior as a scale-free relaxation of the structural elements of the cells and characterizes modifications in the cell mechanical state as changes in the power law exponent. However, MTC also presents limitations. In MTC, cells must be firmly adhered to a substrate to ensure that the stresses applied by the beads deform the cytoskeleton locally and do not move the cell as a whole. However, neutrophil adhesion (which in MTC takes place both with substrate and bead) is known to change the activation state of neutrophils (18) as well as their mechanical properties (4). Passive neutrophils thus cannot readily be probed with existing MTC techniques. Moreover, obtaining the magnitude of  $G^*(\omega)$  from the value of  $g^*(\omega)$  measured with MTC requires knowledge of the degree of microbead embedding, which is difficult to determine.

Atomic force microscopy (AFM) may overcome most of the limitations of the above techniques for probing neutrophil rheology. AFM can obtain  $G^*(\omega)$  of single cells by applying oscillatory indentations to the cell with a microtip attached to a cantilever of a known bending constant and then measuring the resulting force (19). Measurements can be made for oscillations spanning a range of three frequency decades. Moreover, neutrophils can be maintained in a passive state by plating them on substrates rendered almost non-adhesive through coating with poly(HEMA) (20) and by applying only small deformations. Finally and given the geometry of measurements, the use of microspheres as cantilever tips allows the application of the simple two-sphere Hertz contact equation, which has few assumptions and provides a direct estimation of  $G^*(\omega)$ . The use of microspheres with sizes comparable to that of neutrophils also provides a measurement at the whole cell level, which is the length scale of neutrophil dynamics during microvascular circulation.

The aim of this work was thus to measure  $G^*(\omega)$  for passive and activated rat neutrophils with AFM over a broad frequency range. For this purpose, neutrophils were isolated from Sprague-Dawley rats and seeded onto glass slides with a part coated with poly(HEMA), where cells remain almost nonadhered and are thus prevented from activating, and another uncoated part where cells firmly adhere and activate.  $G^*(\omega)$  was measured by indenting the neutrophils with spherical AFM tips and then applying a multi-frequency

signal of 50-nm amplitude with six sinusoidal components of frequencies ranging from 0.1 to 102.4 Hz. The effect of cytoskeletal structure in neutrophil rheology was assessed by disrupting the F-actin cytoskeleton with cytochalasin D. Cell rheological behavior was interpreted by means of the Kelvin body model and the power law structural damping model.

## METHODS

### Isolation of rat neutrophils

Neutrophils were isolated from male Sprague-Dawley rats (Charles River, Wilmington, MA) following a three-step gradient (1.083 mg/ml/1.119 mg/ml) technique (21). All products used in the process were obtained from Sigma (St. Louis, MO) unless otherwise stated. First, rats were anesthetized with pentobarbital sodium (Laboratorios Normon, Madrid, Spain). The blood of the animal was then extracted by cardiac puncture and anticoagulated with sodium citrate 1:9. Next, 7 ml of blood were left to sediment in a solution containing 2/3 (v/v) 3% dextran (0.9% saline solution) for 30 min at room temperature. The buffy coat was then collected and layered on 3 ml of Histopaque 1.083 and 3 ml of Histopaque 1.119 in a Falcon tube, which was centrifuged for 35 min at  $380 \times g$  and  $4^\circ\text{C}$ . The solution present at the interphase between the two Histopaque solutions was then collected, resuspended in 10 ml  $\text{NH}_4\text{Cl}$  0.83% (w/v) (lysis solution, pH 7.4) for 5 min, and centrifuged again for 10 min at  $330 \times g$  and  $4^\circ\text{C}$ . Finally, the pellet obtained was suspended in phosphate buffer saline (PBS), centrifuged for 10 min at  $330 \times g$  and  $4^\circ\text{C}$ , and resuspended with Hanks' balanced salt solution (HBSS). The purity of isolated neutrophils was  $>95\%$ .

### Sample preparation

To prepare glass slides, a stamp (1  $\text{cm}^2$  area) of poly(dimethylsiloxane) (PDMS, Dow Corning, Midland MI) was first placed in conformal contact with a coverslip of 18 mm diameter. A solution (150  $\mu\text{l}$ ) containing 1.5  $\mu\text{g/ml}$  of poly(HEMA) (Sigma) in 95% ethanol was then deposited on the coverslip and left to dry at  $40^\circ\text{C}$  for 3 h. After removing the PDMS stamp, the slide showed a coated portion (corresponding to a rim around the PDMS stamp) and an uncoated portion (corresponding to the zone protected by the PDMS stamp). The used concentration of poly(HEMA) was high enough to prevent neutrophil activation in contact with glass, but low enough that cells would not move freely, allowing thus for AFM measurements. A solution of HBSS containing from  $10^5$  to  $5 \times 10^5$  cells was then placed on the coverslip, incubated for 10 min at room temperature, and rinsed with HBSS. In cytochalasin D experiments, cells were then incubated with cytochalasin D 2  $\mu\text{M}$  (Sigma) for 30 min before AFM measurements. For cell diameter measurements and F-actin imaging, cells were plated in coverslips either completely coated with poly(HEMA) or uncoated without using PDMS stamps.

### AFM measurements

$G^*(\omega)$  of cells was measured with a custom-built AFM attached to an inverted optical microscope (Zeiss Axiovert S 100, Oberkochen, Germany) by using a previously described method (Fig. 1) (19,22). Cells were probed by V-shaped Au-coated silicon nitride cantilevers (nominal spring constant of  $k = 0.01 \text{ N/m}$ ) with a spherical polystyrene bead of radius  $r_1 = 2.25 \mu\text{m}$  glued at their end (Novascan Technologies, Ames, IA). First, the spring constant of the cantilevers was calibrated using the thermal fluctuations method (23,24). Before measurements, the relationship between the photodiode signal and cantilever deflection was calibrated by taking a force-displacement curve at a bare region of the glass coverslip and measuring its slope.

At the time of measurements, the bright-field image from the microscope attached to the AFM was used to position the spherical tip of the cantilever

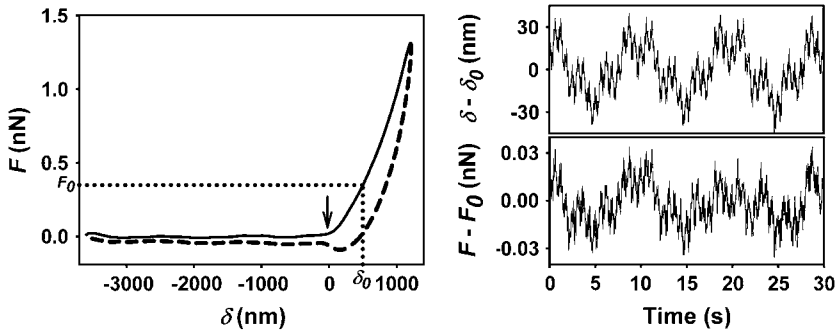


FIGURE 1 Illustration of the measurement method. (Left) Example of a force-indentation ( $F$ - $\delta$ ) curve obtained as the cantilever tip approached and contacted the cell (solid line) and then retracted (dashed line). The curve was then used to determine the contact point between tip and cell (arrow). Starting from the arrow, positive values of  $\delta$  indicate indentation, and negative values indicate tip-cell distance. Once the contact point was determined, the cantilever was placed at an operating indentation ( $\delta_0$ ) of  $\sim 500$  nm and a multi-frequency signal of 50-nm amplitude was applied. (Right) Corresponding multi-frequency indentation (top) and force (bottom) signals used to calculate  $G^*(\omega)$ .

over the central region of a neutrophil. Ten force-displacement ( $F$ - $z$ ) curves (where  $F = kd$ ,  $d$  being cantilever deflection) were obtained by ramping the cantilever in the vertical direction at a constant speed ( $2.5 \mu\text{m}$  amplitude, 1 Hz, indentation  $\sim 1 \mu\text{m}$ ) to determine the zero force offset and the contact point ( $F_c, z_c$ ) between the cell and the cantilever tip. The tip was then placed at an indentation  $\delta = (z - z_c) - d$  of  $\sim 0.5 \mu\text{m}$ , and a small vertical oscillation containing a multi-frequency signal composed of six sine waves (0.1, 0.4, 1.6, 6.4, 25.6, and 102.4 Hz, 50 nm amplitude) was applied for 140 s. Finally, the contact point was determined again as described to account for possible drifts. To determine the viscous drag of the cantilever, three force-displacement curves ( $2.5 \mu\text{m}$  amplitude, 0.1 Hz, maximum indentation  $1 \mu\text{m}$ ) with a superimposed sinusoidal oscillation of 50-nm amplitude and 102.4 Hz were obtained over the cell (25). AFM was also used to evaluate cell height by taking a force curve in a bare region of the coverslip next to the cell. The difference between the contact point between the tip and the substrate and the previously found contact point between the tip and the cell was taken as the cell height. Neutrophils were measured sequentially from the same sample for 1 h, switching randomly between the poly(HEMA)-coated part and the uncoated part. Rounded neutrophils were selected on the coated portion, whereas spread polarized neutrophils were selected on the uncoated portion (both morphologies represented the vast majority of neutrophils in each respective portion).

## Data processing

$G^*(\omega)$  was calculated from AFM measurements as described previously (19,22). Briefly, the contact point  $z_c$  and the apparent Young's modulus  $E$  were determined by least squares fitting of the Hertzian force-indentation relationship of a spherical punch with infinite stiffness indenting an elastic sphere (26):

$$F = \frac{4E}{3(1-\nu^2)} R^{1/2} ((z - z_c) - d)^{3/2} = \frac{4E}{3(1-\nu^2)} R^{1/2} \delta^{3/2}, \quad (1)$$

where  $\nu$  is the Poisson ratio (assumed to be 0.5) and  $1/R = 1/r_t + 1/r_n$ , with  $r_t = 2.25 \mu\text{m}$  being the radius of the spherical cantilever tip and  $r_n$  being the average neutrophil radius. For each cell,  $E$  and  $z_c$  were taken as the average of the values determined from the force-displacement curves obtained before and after the multi-frequency oscillations. Once the contact point was determined, force-displacement curves were also used to obtain the value predicted for  $E$  from Eq. 1 as a function of indentation to evaluate whether the measurements were affected by the underlying substrate (22). Equation 1 can be approximated for oscillations around an operating indentation  $\delta_0$  by taking the first term of the Taylor expansion. Expressing, then, Eq. 1 in terms of the shear modulus  $G = E/2(1 + \nu)$  and converting to the frequency domain (19),

$$G^*(\omega) = \frac{1-\nu}{4R^{1/2}\delta_0^{1/2}} \left( \frac{F(\omega)}{\delta(\omega)} - iw b(0) \right), \quad (2)$$

where  $\omega = 2\pi f$  is the angular frequency and  $iwb(0)$  is the correction for the viscous drag force exerted by the liquid medium on the cantilever. The viscous drag factor  $b$  was calculated at different heights from the cell surface and extrapolated to the cell surface ( $b(0)$ ) by analyzing the noncontact parts of the curves as described in Alcaraz et al. (25).  $G^*(\omega)$  was expressed in terms of its real and imaginary parts as  $G^* = G' + iG''$ , with  $G'$  and  $G''$  being the elastic and loss moduli, respectively.

## Immunofluorescence and optical microscopy

To observe the organization of the F-actin cytoskeleton, cells were fixed with 4% formaldehyde in PBS, incubated with Phalloidin-Tetramethylrhodamine (Sigma), and then visualized with a charge-coupled device camera (ORCA-AG, Hamamatsu, Morimoto, Japan) attached to an inverted optical microscope (Eclipse TE 2000 microscope, Nikon, Tokyo, Japan) using a  $60\times$  objective. Sample manipulation and rinsing were done with extreme care to prevent detachment of cells from poly(HEMA) substrates. Live cells were also visualized with phase contrast ( $10\times$ ) and differential interference contrast (DIC,  $60\times$ ) microscopy using the same microscope. Phase contrast images were also used to measure mean cell diameters after visual identification.

## Modeling

### Liquid droplet and Kelvin models

In some studies, leukocytes have been modeled as a liquid droplet consisting of a cortex with cortical tension  $T$  enclosing either a viscous Newtonian liquid (with viscosity  $\mu_N$ ) (8,9,12) or a viscoelastic Maxwell liquid (represented by a spring constant  $k_M$  in series with a dashpot with viscosity  $\mu_M$ ) (10,13). In other studies, leukocytes have been modeled as a whole as a standard viscoelastic or Kelvin body, with two springs  $k_{S1}$  and  $k_{S2}$  and a dashpot  $\mu_S$  (11,14) (Fig. 2). The complex shear modulus of a Kelvin body can be expressed as (27)

$$G_K^*(\omega) = k_{S1} + \frac{\mu_S^2 k_{S2} \omega^2}{k_{S2}^2 + \mu_S^2 \omega^2} + i \frac{\mu_S k_{S2} \omega}{k_{S2}^2 + \mu_S^2 \omega^2}. \quad (3)$$

It is, however, less straightforward to fit liquid droplet models to the data, as force-indentation data were processed considering the cell as a single body and without distinguishing between cortex and interior. This distinction can be made by considering that the cell cortex exerts a force on the spherical tip which is calculated as (28)

$$F_{\text{membrane}} = \frac{2T}{r_t} \pi a^2, \quad (4)$$

where  $a$  is the contact radius between the tip and the cell, which is related to the indentation  $\delta$  as  $a^2 = \delta R$  for small indentations (26). Neglecting cortex

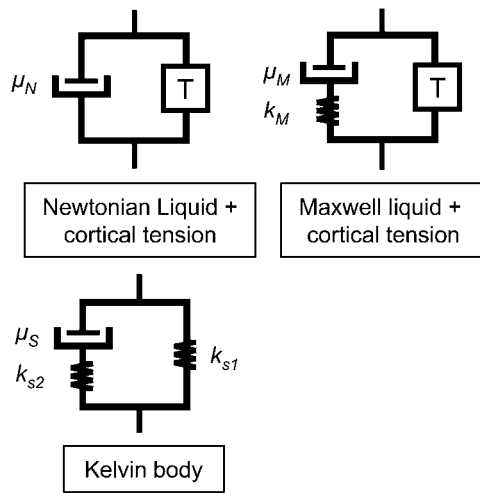


FIGURE 2 Mechanical models commonly used to interpret leukocyte rheology. The Newtonian liquid droplet model is composed of a cell cortex with cortical tension  $T$  enclosing a Maxwell liquid droplet with viscosity  $\mu_N$ . In the Maxwell liquid droplet model, the cell cortex encloses a viscoelastic liquid (represented by a spring  $k_M$  in series with a dashpot  $\mu_M$ ). In the Kelvin model, cortex and cell interior are represented as a viscoelastic body composed of a spring  $k_{S1}$  in parallel with a series combination of a spring  $k_{S2}$  and a dashpot  $\mu_S$ . For the small indentations used in this study, the cortical tensions in parallel present in the liquid droplet models can be considered as springs (see Methods).

thickness, the total force on the cantilever is the sum of the forces exerted by the cortex and the cell interior:

$$F = \frac{4E_i}{3(1-\nu^2)} R^{1/2} \delta^{3/2} + \frac{2T}{r_i} \pi \delta R, \quad (5)$$

where  $E_i$  is the Young's modulus of the interior of the cell. Equating Eq. 1 with Eq. 5, we can relate  $E$  as calculated in the data processing section with the liquid droplet model parameters. After expressing in terms of  $G$ , approximating around an indentation point  $\delta_0$ , and converting to the frequency domain, it can be seen that

$$G_{NM}^*(\omega) = G_i^*(\omega) + k_T, \quad (6)$$

where

$$k_T = \frac{\pi(1-\nu)}{2r_i} \left( \frac{R}{\delta_0} \right)^{1/2} T. \quad (7)$$

$G_{NM}^*(\omega)$  in Eq. 6 corresponds to the liquid droplet model prediction of the measured  $G^*(\omega)$  (defined in Eq. 2), which in this model should be equal to the sum of  $G_i^*(\omega)$  (the complex shear modulus of the cell interior) and a frequency-independent term  $k_T$  given by cortical tension. For the purposes of this study, the cortical tension present in the liquid droplet models can be considered as a spring in parallel to the cell interior with spring constant  $k_T$ . Note that  $k_T$  depends on the specific measurement conditions and is thus a function of  $\delta_0$ ,  $r_i$ , and  $r_n$ . The Maxwell liquid droplet model becomes, thus, equivalent to the Kelvin model with  $k_{S1} = k_T$ . The Newtonian liquid droplet model becomes a particular case of the Kelvin model with  $k_{S1} = k_T$  and  $k_{S2} = \infty$  (Fig. 2). Given that the Kelvin model (with  $G^*(\omega)$  defined in Eq. 3) comprises all other models, it was chosen to fit the data. Equation 3 was also used to estimate values of  $G^*(\omega)$  from previous publications reporting parameters obtained with liquid droplet or Kelvin models from micropipette aspiration tests in leukocytes. To estimate  $G^*(\omega)$  from works using Newtonian and Maxwell liquid droplet models, values of  $r_i = 2.25 \mu\text{m}$ ,  $\delta_0 = 0.5 \mu\text{m}$ , and the mean  $r_n$  obtained in this study were used to calculate  $k_T$ .

### Power law structural damping model

The power law structural damping model describes  $G^*(\omega)$  as (29)

$$G_{SGR}^* = G_0 \left( \frac{\omega}{\Phi_0} \right)^{x-1} (1 + i\eta) \Gamma(2-x) \cos \frac{\pi}{2}(x-1) + i\omega\mu, \quad (8)$$

where  $G_0$  and  $\Phi_0$  are scaling factors for stiffness and frequency, respectively,  $\eta = \tan((x-1)\pi/2)$  is the hysteresivity or structural damping coefficient,  $x-1$  is the power law exponent, and  $i\omega\mu$  is an additional Newtonian viscous term. In the model,  $x=1$  corresponds to a purely elastic solid, and  $x=2$  corresponds to a Newtonian liquid. This equation predicts a scale-free power law behavior of both  $G'$  and  $G''$  and a coupling between them ( $G'' = \eta G'$ ) at low frequencies (where  $i\omega\mu$  is small). It has been reported that  $\Phi_0$  can be assumed to be constant within a given cell type, and even across cell types (16,30,31). We therefore took  $\Phi_0 = 2.5 \times 10^8 \text{ rad/s}$ , a value which has been shown to provide an adequate fit for many cell types, including neutrophils (29). Equation 8 was fitted independently to  $G^*(\omega)$  data for each cell condition (on poly(HEMA) or on glass and with or without cytochalasin D).

Fits to the data for the Kelvin and structural damping models were done for the mean values of  $G^*(\omega)$  for each cell condition. Fits were obtained by minimizing the sum of squares of the differences between the logarithm of  $G^*(\omega)$  and that of the predictions of the models (Eqs. 3 and 8) (31). Software developed in MATLAB (The MathWorks, Natick, MA) using a nonlinear least-squares trust-region algorithm was used for fitting.

### Statistics

Data are shown as mean  $\pm$  SE for neutrophils extracted from  $n = 6$  rats ( $G^*(\omega)$  of untreated cells and cell height data) or  $n = 3$  rats ( $G^*(\omega)$  of cytochalasin D treated cells and cell diameter data). For each rat and condition, data were taken as the average of all measured neutrophils ( $\sim 4$  neutrophils per rat and condition for  $G^*(\omega)$  and cell height data and 15 for cell diameter data). The combined effects of activation and cytochalasin D on  $G'$  at 1.6 Hz were analyzed with two-way analysis of variance. Cell heights and diameters and correlation coefficient ( $r^2$ ) values obtained from Kelvin and structural damping fits were analyzed with Student's  $t$ -tests. All analyses were performed with SigmaStat software (Systat Software, Richmond, CA). Statistical significance was assumed at  $p < 0.05$ .

### RESULTS

Differences were found between neutrophils depending on whether they were allowed to adhere to their substrate or not. On the one hand, neutrophils on poly(HEMA) had a diameter of  $8.15 \pm 0.33 \mu\text{m}$  and a height of  $4.95 \pm 0.47 \mu\text{m}$  and most showed a rounded shape (Fig. 3). These cells did not adhere firmly (as they could be removed from the coverslip by means of a few rinses) and showed a mainly cortical and nonpolar F-actin organization. On the other hand, neutrophils firmly adhered to bare glass had a larger diameter ( $13.19 \pm 0.90 \mu\text{m}$ ,  $p < 0.01$ ) and a lower height ( $3.62 \pm 0.32 \mu\text{m}$ ,  $p < 0.05$ ). The shape of neutrophils on glass was generally less rounded and more polarized and allowed us to distinguish between a lamellipodium and a uropod (usually referred to as leading and trailing edges). Moreover, F-actin organization was polarized on cells plated on glass, with a clear accumulation on the lamellipodium.

Round neutrophils on poly(HEMA) had a mean value of  $E = 893 \pm 275 \text{ Pa}$ . The dependence of  $E$  on indentation was

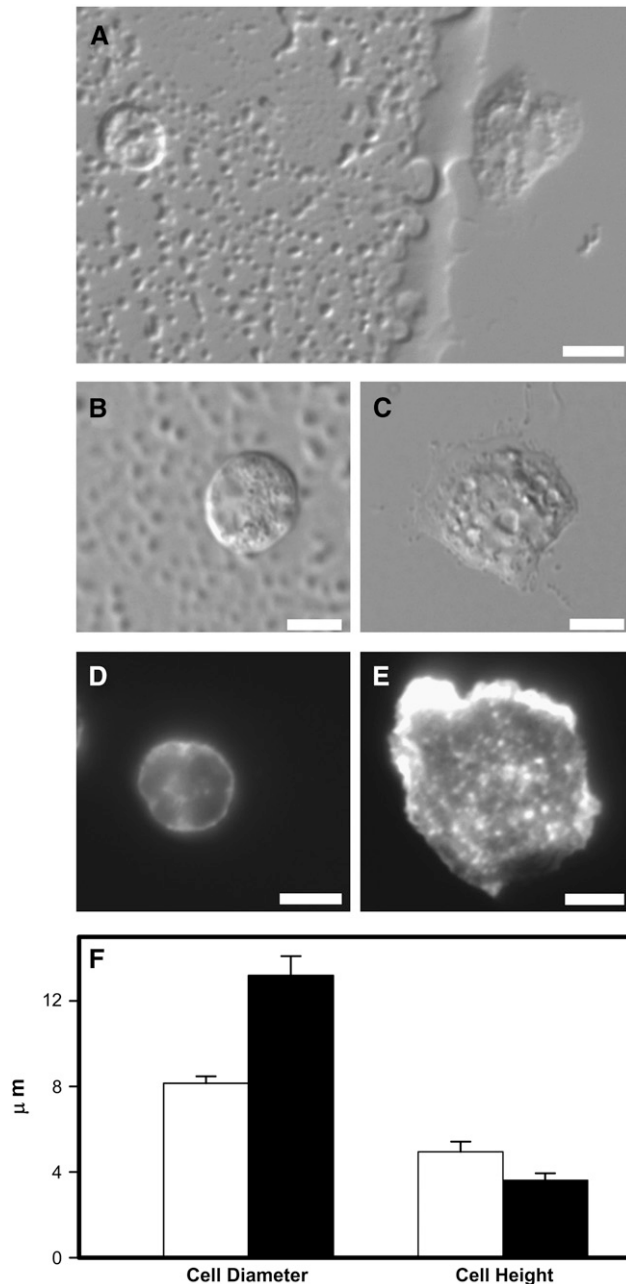


**FIGURE 3** Differences between neutrophils plated on poly(HEMA) and glass. (A) DIC image showing the border between the portion coated with poly(HEMA) (*left*) and the uncoated part (*right*). A neutrophil can be seen in each of the portions, with the cell on glass being larger and less rounded. (B and C) Magnified DIC image of a neutrophil on poly(HEMA) (B, *left*) and on glass (C, *right*). (D and E) Immunofluorescence images of F-actin of a neutrophil on poly(HEMA) (D, *left*) and glass (E, *right*). The leading edge with an accumulation of F-actin is clearly visible in the cell on glass, and the cell on poly(HEMA) shows a more uniform distribution of F-actin. (F) Mean cell diameter and height of neutrophils on poly(HEMA) (*open bars*) and glass (*solid bars*).

evaluated for the obtained force-displacement curves (Eq. 1). The results showed that  $E$  (and thus  $G^*(\omega)$ ) was independent of indentation around the operating point  $\delta_0 = 500$  nm (Fig. 4). The working indentation was thus high enough to be beyond the contact zone, where  $E$  is misestimated (22), and low enough to prevent substrate effects (which lead to an overestimation of  $E$  (32)).

The changes observed in neutrophil morphology and cytoskeletal organization were associated with changes in rheology. At 1.6 Hz, round neutrophils on poly(HEMA) had  $G' = 380 \pm 121$  Pa, whereas spread neutrophils on glass showed a higher mean  $G'$  value of  $909 \pm 135$  Pa ( $p < 0.05$ ). Similar changes were found in  $G'$  and  $G''$  for all frequencies (Fig. 5). The frequency dependence of  $G'$  and  $G''$  for neutrophils on both poly(HEMA) and glass followed a scale-free behavior with a value for  $\eta$  which was nearly constant for the lower frequencies (Fig. 5). When neutrophils were exposed to cytochalasin D to disrupt the actin cytoskeleton, the scale-free behavior was maintained (Fig. 6), and  $G'$  decreased significantly at 1.6 Hz by 64% for cells on glass ( $p < 0.05$ ) but not significantly (51%) for cells on poly(HEMA).  $G''$  for cytochalasin D treated cells followed a similar behavior (Fig. 6).

Adjusting the Kelvin model (Eq. 3) to  $G^*(\omega)$  data resulted in poor fits ( $r^2 = 0.534$  for cells on poly(HEMA) and  $r^2 = 0.334$  for cells on glass). By contrast, structural damping model fits (Eq. 8) were excellent (Table 1) with  $r^2$  values significantly higher than those of the Kelvin model when  $G^*(\omega)$  data were fitted separately for each rat ( $p < 0.001$ ). The parameter  $x$ , indicative of the slope of the fitted power law, was higher for cells plated on poly(HEMA) than for

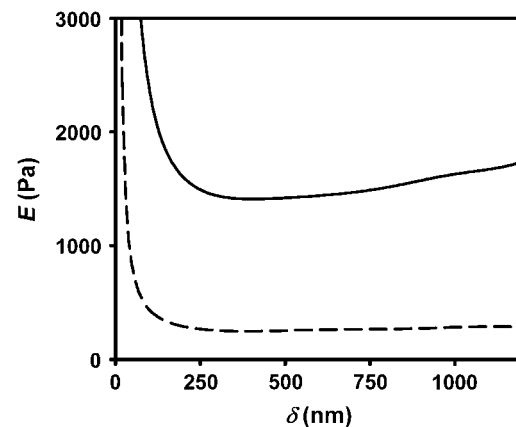


**FIGURE 4** Effect of cell thickness on the determination of the apparent Young's modulus  $E$ . Plots showing the Hertz contact model calculation of  $E$  as a function of indentation for representative force-displacement curves of a very thin cell on glass (*solid line*, 2066-nm thickness) and a thick cell on poly(HEMA) (*dashed line*, 5591-nm thickness). The plateau observed for the thick cell indicates that there is no substrate effect. Substrate effects for the thin cell (observed as an increase in  $E$  as a function of indentation) only become important at indentations higher than the working indentation ( $\sim 500$  nm).

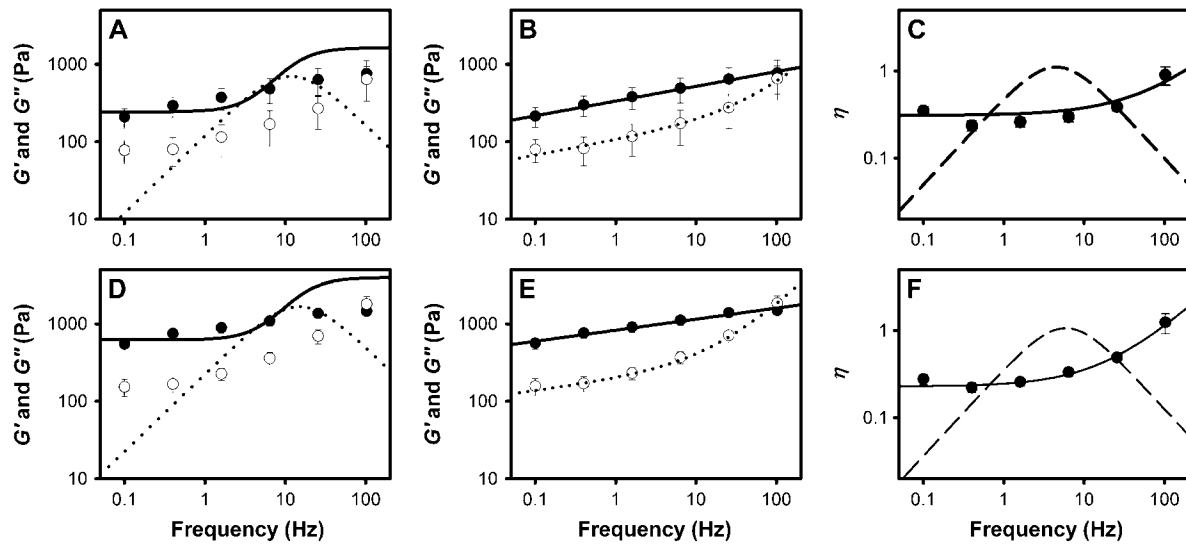


FIGURE 5 Dependence of  $G^*(\omega)$  on frequency and activation. (A and B) Measured  $G'$  (solid symbols) and  $G''$  (open symbols) for neutrophils on poly(HEMA). Solid and dotted lines represent, respectively, the best fits for  $G'$  and  $G''$  of the Kelvin model (A) and the power law structural damping model (B). (C) Corresponding values of  $\eta$  for measured data (solid symbols), the Kelvin model fit (dashed line), and the power law structural damping model fit (solid line). (D–F) Same data for neutrophils on glass.

cells on glass, with nonoverlapping confidence intervals. The Newtonian viscous term  $\mu$  was higher for cells on glass than for cells on poly(HEMA), also with nonoverlapping confidence intervals. However,  $G_0$  was very similar for both states with overlapping confidence intervals. The fits of the structural damping equation to cells treated with cytochalasin D showed a decrease in  $G_0$  and  $x$  with respect to untreated cells. These parameters were similar for treated cells on both poly(HEMA) and glass, with overlapping confidence intervals.

$G^*(\omega)$  data for passive neutrophils are compared in Fig. 7 with values of  $G^*(\omega)$  predicted by taking the liquid droplet or Kelvin model parameters reported in different micropipette aspiration studies and using them in Eq. 3 as described in

Methods. These values correspond to the  $G^*(\omega)$  that the models predict for our particular measurement conditions and are therefore dependent on  $\delta_0$ ,  $r_t$ , and  $r_n$ . The measured  $G'$  was considerably higher than values predicted from the micropipette aspiration studies. Moreover, the frequency dependence and values of both  $G''$  and  $\eta$  predicted from the micropipette studies were very different from the values measured in this study.

## DISCUSSION

We used AFM to measure the complex shear modulus of rat neutrophils from 0.1 to 102.4 Hz for passive cells and cells

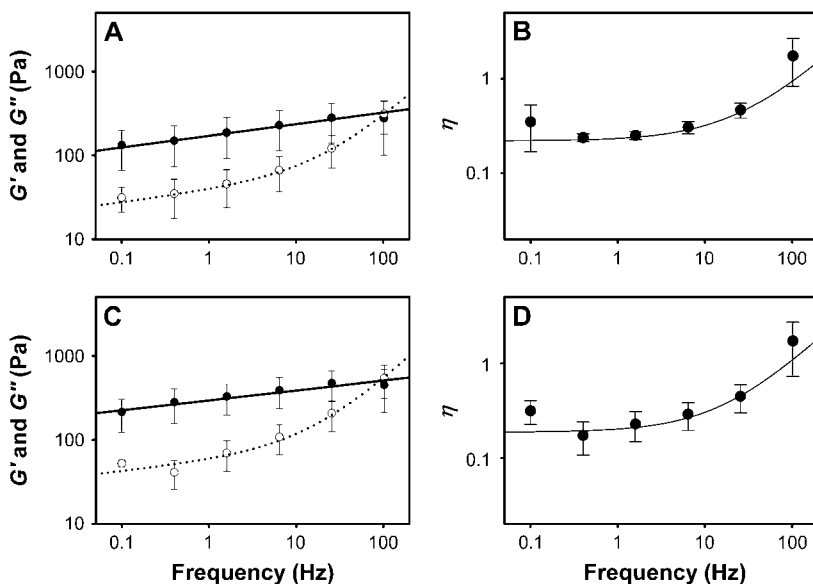


FIGURE 6 Dependency of  $G^*(\omega)$  on cytochalasin D treatment. (A and B) Measured values for neutrophils treated with cytochalasin D on poly(HEMA) of  $G'$  and  $G''$  (A, solid and open symbols, respectively) and  $\eta$  (B, solid symbols). (C and D) Same data for treated cells on glass. Plotted lines represent the best fits of the structural damping model.

**TABLE 1 Comparison of fitted structural damping parameters for the different experimental conditions used (bold font)**

Treatment	Substrate	$G_0$ (Pa)	$x$	$\mu$ (Pa.s)	$r^2$
No treatment	Poly(HEMA)	<b>11071</b> <i>7940–14203</i>	<b>1.184</b> <i>1.167–1.201</i>	<b>0.616</b> <i>0.461–0.771</i>	<b>0.996</b>
	Glass	<b>13596</b> <i>10389–16802</i>	<b>1.148</b> <i>1.134–1.163</i>	<b>2.321</b> <i>1.951–2.690</i>	<b>0.991</b>
Cytochalasin D	Poly(HEMA)	<b>2368</b> <i>1752–2985</i>	<b>1.139</b> <i>1.123–1.155</i>	<b>0.376</b> <i>0.301–0.451</i>	<b>0.982</b>
	Glass	<b>2785</b> <i>1649–3921</i>	<b>1.112</b> <i>1.09–1.143</i>	<b>0.743</b> <i>0.515–0.971</i>	<b>0.978</b>

Italic subscripts indicate the lower and upper bounds of the corresponding 95% confidence intervals.

activated through adhesion. Rheology of both passive and adhered neutrophils revealed a scale-free behavior of  $G^*(\omega)$ , which increased with frequency as a weak power law and showed a coupling between elastic and loss moduli. Passive neutrophils exhibited an elastic modulus at low frequencies of  $\sim 350$  Pa with a loss modulus  $\sim 4$ -fold smaller and a power law exponent of  $\sim 0.2$ . Adhered neutrophils were over twofold stiffer and had a smaller power law exponent, indicative of a more solid-like behavior. Disruption of the actin cytoskeleton with cytochalasin D resulted in softer but more solid-like cells. The Kelvin model was unable to account for the scale-free behavior. By contrast, the power law structural damping model captured the most important features of neutrophil rheology.

AFM allowed us to measure  $G^*(\omega)$  of neutrophils with minimal cell perturbation by indenting cells with microsphere probes attached to the cantilever end. The use of microspheres instead of the more common pyramidal tips served different purposes. First, it minimized the slipping of the loosely adhered neutrophils on poly(HEMA) when squeezed by the tip, which permitted us to perform stable measurements without having to physically confine non-adhered cells as done previously (33,34). Second, the diameter of the used microspheres ( $4.5 \mu\text{m}$ ) is comparable to that of neutrophils, which implied that measurements were done at the whole cell level. Additionally, the large diameter of the microspheres allowed us to neglect the role of cortex bending stiffness (35), thereby discarding the effects of this parameter in the interpretation of the results with liquid droplet models. Finally, the use of microspheres allowed us to approximate tip-cell contact with the simple Hertz contact equation between two spheres (cantilever tip and neutrophil). It should however be noted that the force applied by the tip also causes a small deformation of the neutrophil at the cell-substrate interface, resulting in a slightly underestimated  $G^*(\omega)$ . We modeled neutrophils as spheres with a constant diameter taken as the mean diameter of passive neutrophils as observed with phase contrast microscopy. This option was chosen for simplicity and because the effect of this parameter on  $G^*(\omega)$  computation is relatively small. In the extreme case of considering the cells as semiinfinite planes, for example, the resulting increase in  $R$  would only imply a 24% decrease

in  $G^*(\omega)$  (Eq. 2). With respect to the measurement process, we used an operating indentation of  $\sim 500$  nm with a superimposed multi-frequency oscillation of 50-nm amplitude. This indentation depth was high enough to prevent the uncertainty in  $G^*(\omega)$  present near the contact point (22) but low enough to minimize substrate effects (Fig. 4) and to ensure that measurements were done in the range where the Hertz contact equation is valid (36). These last two assumptions are confirmed by the observed plateau in  $E$  around the working indentation, even for the thinnest cells. Moreover, earlier work showed that our range of cell thicknesses could only have had a small effect in  $G^*(\omega)$  determination (32). The indentation used was also selected to be small enough to prevent a mechanical activation of the neutrophils. Indeed, deformations of neutrophils of up to  $\sim 3 \mu\text{m}$  (when passing through  $5\text{-}\mu\text{m}$ -diameter pores) have been observed not to activate neutrophils (15). Regarding the multi-frequency measurements, the oscillations applied to the cells simultaneously provided measurements at different frequencies, minimizing the problems associated with cantilever drifts or cell movement. No cross talk between frequencies was noted as concluded after observing that 99.5% of the energy of the spectral response of cells to a 0.1-Hz sinusoidal signal was contained in this same frequency (data not shown).

Cells plated on glass coverslips coated with poly(HEMA) showed important morphological and cytoskeletal differences with respect to cells plated on uncoated coverslips. Poly(HEMA) is a polymer coating used to prevent cell adhesion to substrates (20). However, neutrophils on poly(HEMA) were loosely adhered to the substrate. Although this weak adhesion could reflect a small degree of activation, cells on poly(HEMA) were considered to be passive according to their morphological and cytoskeletal characteristics (a round appearance with no visible protrusions and a nonpolar F-actin distribution). On the other hand, the formation of a lamellipodium and a uropod as well as the accumulation of F-actin in the leading edge (all observed in adhered cells plated on glass) are characteristics associated with neutrophil adhesion to the endothelium in immune responses (2). Moreover, the changes in cell spreading observed in the two cases have also been described to occur in leukocyte adhesion to the endothelium (37,38). Plating cells on glass seems thus to

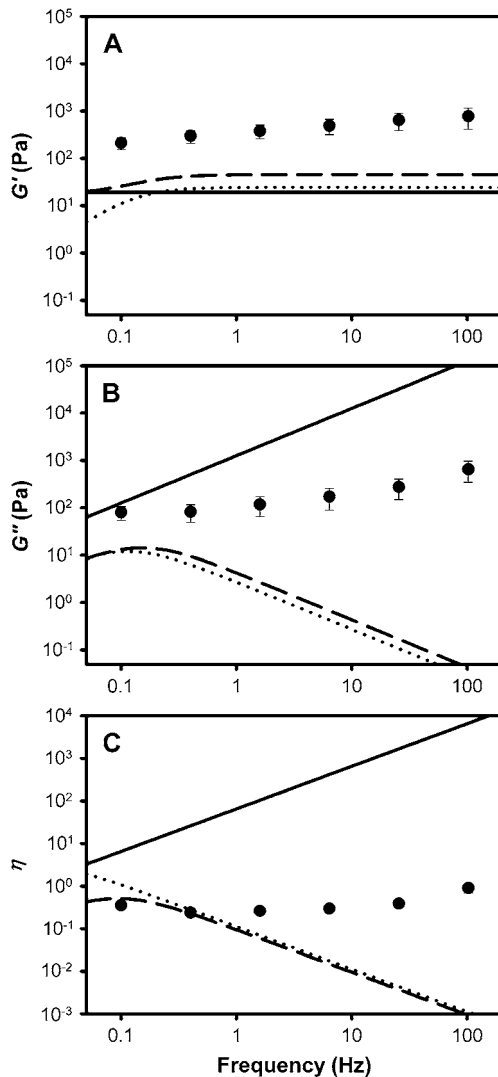


FIGURE 7 Comparison of measured  $G^*(\omega)$  for neutrophils on poly (HEMA) with predictions obtained from the liquid droplet and Kelvin model parameters reported in different studies. Measured values of  $G'$ ,  $G''$ , and  $\eta$  (solid symbols in A, B, and C, respectively) are plotted with the Newton model prediction from Evans and Yeung (8) (solid lines), the Maxwell model prediction from Dong et al. (10) (dashed lines), and the Kelvin model prediction from Sung et al. (11) (dotted lines).

induce a neutrophil response which has elements in common with the physiological activation of neutrophils adhered to the endothelium. We thus took round neutrophils on poly(HEMA) and adhered neutrophils on glass as models of passive and activated neutrophils, respectively.

To our knowledge, this study provides the first measurements of  $G^*(\omega)$  as a function of frequency of passive whole neutrophils. Our results showed that  $G^*(\omega)$  was scale free at the frequencies probed and that both  $G'$  and  $G''$  (and thus also cell stiffness) increased with frequency. These findings for the frequency dependence thus extend the results found in activated neutrophils by Fabry et al. (16) with MTC to passive neutrophils. The increase in stiffness with frequency

observed in this study for small deformations has also been reported for large deformations with AFM (33). Additionally and for the low frequencies,  $\eta$  was approximately constant with a value of  $\sim 0.3$ , which is indicative of a coupling between elastic and loss components. These results resemble those obtained with several types of adherent cells (19,29,39) and show that neutrophils and adherent cells have more similar rheological properties than previously believed. Although no former measurements of  $G^*(\omega)$  for passive neutrophils exist, our value of  $E$  estimated from  $F$ - $z$  curves ( $\sim 900$  Pa) falls in the broad range of previously reported data (200–1400 Pa) (4,5,33,40). Our study showed that  $G^*(\omega)$  was higher for adhesion-activated cells, which is probably due to an increase in F-actin polymerization (Fig. 3) caused by activation (4). The higher  $G^*(\omega)$  of activated cells could also be explained by an increase in membrane tension caused by adhesion (41). However, a high membrane tension should have been associated with a failure of the Hertz force-indentation relationship, which was not observed (Fig. 4). That the F-actin cytoskeleton regulates the observed mechanical response to activation is also sustained by the fact that disrupting F-actin with cytochalasin D was associated with a smaller decrease in  $G^*(\omega)$  in passive cells than in activated ones. Results from former studies stimulating leukocytes either with fMLP or by adhesion to the endothelium and using MTC (16,42), cell pocker (4), and micropipette aspiration (14) also showed an increase in stiffness with activation. Interestingly, results obtained by tracking the motion of endogenous granules (43) showed a decrease in stiffness of the neutrophil cytoplasm after mechanical activation caused by the large deformation of cells into 3- $\mu\text{m}$  pores. This could reflect differences in the response of neutrophils to mechanical stimulation with respect to activation through adhesion or fMLP or differences in the mechanical response of the cytoplasm with respect to that of the actin-rich cortex. These two cell regions could exhibit different mechanical properties. Indeed, values for  $G^*$  of the cytoplasm of activated neutrophils reported with optical tweezers (OT) at  $\sim 1$  Hz (44) were two orders of magnitude lower than our values. This difference, together with the small expected contribution of the nucleus to our measurements given by the small indentations used, suggests that the global mechanical properties of neutrophils measured in this study were dominated by the cell cortex. The neutrophil cortex would then show viscoelastic scale-free dynamics and not a purely elastic behavior as previously considered.

The Kelvin model (Eq. 3) was not able to reproduce measured  $G^*(\omega)$  data. We only fitted this model and not liquid droplet models since these can be regarded as particular cases of the Kelvin model for our experimental setup if cortex thickness is neglected (see Methods). For our comparative purposes this is a reasonable assumption as the cortex thickness is generally considered to be of  $\sim 0.1 \mu\text{m}$  (35) and thus much smaller than the indentation depth (0.5  $\mu\text{m}$ ). The Kelvin model is characterized by two plateaus

for  $G'$  at low and high frequencies, a peak in  $G''$  between the plateaus, and no energy dissipation in frequencies away from the peak (Fig. 5). None of these features were observed in our data, which resulted in a very poor fit of the model to  $G^*(\omega)$  of both passive and activated neutrophils. Moreover, the magnitude and frequency dependence of  $G^*(\omega)$  predicted by the liquid droplet or Kelvin parameters taken from different micropipette aspiration tests did not agree with the measured values. Although this discrepancy might arise from differences in cell types and species, important disagreements were also found in  $\eta$ . The measured  $\eta$  at low frequencies for passive neutrophils was approximately constant and of  $\sim 0.3$ , which is of the order of measured values in several cell types (19,29,30). However, the predictions from liquid droplet and Kelvin models showed a strong frequency dependence and could be several orders of magnitude below or above measured values (Fig. 7). This seems to indicate that the commonly used combinations of springs and dashpots cannot explain the measured  $G^*(\omega)$ . To further confirm this,  $G^*(\omega)$  was fitted with an expansion of the Kelvin model in which a dashpot was added in series to  $k_{S1}$  to account for cortex viscoelasticity. Even though this model has two time constants, the quality of the fit remained significantly poorer than that of the structural damping fit ( $r^2 = 0.708$  for cells on poly(HEMA) and 0.583 for cells on glass,  $p < 0.001$ ). Both the liquid droplet and the Kelvin models have nevertheless been used successfully to describe leukocyte behavior in micropipette aspiration experiments. An explanation for this apparent discrepancy is that micropipette aspiration experiments generally measure the cell creep response (cell deformation as a function of time given a constant aspiration pressure). The predictions for the creep function of the liquid droplet and Kelvin models are either exponential or linear functions, which can be difficult to distinguish from a power law behavior if the range of time-scales or frequencies is limited, as is the case in most micropipette aspiration experiments. Fitting power law data over a narrow frequency range using models with a reduced number of springs and dashpots will provide values for the fitted parameters with time constants of the order of the timescales of the measurement. Indeed, calculating the time constants of the models as  $t_c = \mu/k$  (with  $\mu$  and  $k$  being any of the springs and dashpots in the models), the values obtained from different micropipette aspiration tests (9,11,13) are of the order of  $10^0$ – $10^1$  s. These values agree with the timescales of most micropipette aspiration tests. The fit of the Kelvin model to our data, on the other hand, provides time constants of the order of  $10^{-2}$  s, which reflects the scale of our wider frequency range.

The power law structural damping model (Eq. 8) reproduced  $G^*(\omega)$  of whole neutrophils very accurately in all cases. A power law rheology has also been reported for the neutrophil cytoplasm. Tsai et al. (45) reported from high deformation micropipette aspiration tests that cytoplasmic viscosity increased with shear rate as a power law, which is

consistent with a similar frequency dependency of cytoplasmic  $G''$ . Recently, a power law structural damping behavior for the cytoplasm of adherent neutrophils was observed by Yanai et al. after displacing intracellular granules with OT (44). Interestingly, the value of  $x \sim 1.5$  obtained with OT was remarkably higher than the figures found for whole neutrophils in this study with AFM ( $x \sim 1.15$ ) and by Fabry et al. with MTC ( $x \sim 1.20$ ) (16). These differences suggest that the cytoplasm is more liquid-like than the actin-rich cortex, which as we argued above is probably the cell component that accounts for most of the mechanical response in AFM and MTC measurements. The power law rheology observed in neutrophils with MTC has been interpreted with the theory of SGR (17,29). SGR features cell rheology as a scale-free relaxation of structural elements of the cell, which are bound by weak interactions and trapped in energy wells with energies higher than thermal agitation. SGR understands the parameter  $x$  as an effective temperature that regulates the probability of the elements of hopping between wells and determines the cell mechanical state between an elastic solid ( $x = 1$ ) and a viscous liquid ( $x = 2$ ). Interestingly, results obtained with MTC for several adherent cell types showed that the modifications in  $G^*(\omega)$  produced by many different pharmacological treatments could be modeled by adjusting only  $x$  and leaving all other parameters fixed (16,31,39). Consistently, the activation-induced stiffening resulted in a decrease in  $x$  without changing  $G_0$  (Table 1), supporting the idea that neutrophil rheology is similar to that of adherent cells. However, when cytochalasin D was applied to disrupt the actin cytoskeleton, the observed cell softening was associated with a reduction in  $G_0$  and  $x$  for both passive and activated neutrophils. A decrease in cytoplasmic stiffness not paralleled by an increase in  $x$  was previously reported by Yanai et al. (44). By contrast, Fabry et al. (16) reported a higher  $x$  after cytochalasin D treatment, in agreement with results obtained with adherent cell types. It should however be noted that the fitting used by Fabry et al. imposed a single value of  $G_0$  for all treatments. This procedure might have resulted in an increased  $x$  caused by the decreased stiffness rather than by the power law slope. Indeed, when we imposed a single  $G_0$  for all treatments (and not one per treatment), the fitted  $x$  for cytochalasin D treated cells rose, even though the quality of the fit was reduced (data not shown). Further work is needed to ascertain the different effect of cytochalasin D on the rheology of neutrophils and adherent cells.

The observed power law rheology of neutrophils could help to better understand the implications of cell mechanics in neutrophil function in the microcapillary circulation. In the pulmonary microcapillary circulation, neutrophils (with diameters ranging from 6 to 8  $\mu\text{m}$ ) must cross 40–100 capillary segments when circulating from arterioles to venules (1). The time neutrophils take to deform into microcapillaries that have diameters smaller than their own is determined by neutrophil rheology (4) and is believed to regulate their adhesion to the endothelium and subsequent migration into

the damaged tissue. Passage from arterioles to venules lasts from 1 s to over 20 min (46). This range is probably given by the different times it takes for neutrophils to deform into differently sized individual capillaries, which have diameters ranging from 2 to 15  $\mu\text{m}$  (1). Considering the number of segments crossed, the timescale of neutrophil deformation in individual capillaries might span from a few milliseconds to minutes. The understanding of the passage of neutrophils through microcapillaries thus requires knowledge of cell mechanics for the wide range of timescales or frequencies involved. As seen in this work for small deformations,  $G'$  increases over 3-fold and  $G''$  over 10-fold when frequency is increased from 0.1 to 100 Hz, making the cell stiffer and more viscous. Even though the magnitude of  $G^*(\omega)$  might vary for high deformations, the power law behavior and the increase in stiffness with frequency seem to be maintained (33,45). Given that the scale-free frequency dependence is not predicted by liquid droplet or Kelvin models, simulations using these models (47,48) will probably only be valid at the timescale of the measurements from which the parameters were derived. The observed power law behavior of  $G^*(\omega)$  could also help to explain neutrophil dynamics in arrest and transmigration. Although the initial process of deformation and arrest takes place fast as the neutrophil hits the capillary at over 100  $\mu\text{m/s}$  (49), transmigration occurs at a slower rate. A fast deformation process implies a high stiffness, which would facilitate neutrophil arrest at the capillary entrance and subsequent adhesion. On the other hand, cell softening for slow deformations would smooth the progress of neutrophil transmigration. Cell rheology might also mediate neutrophil rolling and adhesion to the vascular endothelium in the systemic circulation. Once neutrophils establish an initial molecular bond with the endothelium through the selectin family of adhesion proteins, shear stress in the blood vessel exerts a torque which increases the contact area between the cell and the endothelium (7). The adhesion strength to the endothelium (which determines whether the cell will sequester or not) depends on this contact area, which increases with cell deformability (5,6). The initial adhesive contact between neutrophils and the endothelium slows down the cell and prolongs the timescale of shear stress application. This increases cell deformation and contact area, which could facilitate adhesion to the endothelium and vascular transmigration.

In conclusion, we used an AFM technique which readily allowed us to measure  $G^*(\omega)$  for passive and activated neutrophils, for a broad frequency range, and with minimal cell perturbation.  $G^*(\omega)$  increased with frequency as a weak power law. The measured neutrophil rheology appears to be dominated by the cell cortex, which would then exhibit a power law behavior and not a purely elastic response. The scale-free dynamics conformed to the power law structural damping model but not to liquid droplet and Kelvin models. In accordance with results obtained on adherent cell types, the stiffening induced by activation could be modeled by

simply reducing the power law slope. However, the effect of cytoskeleton disruption with cytochalasin D on the power law slope seems to be different in neutrophils and adherent cells. The increase in stiffness with frequency may modulate neutrophil transit, arrest, and transmigration in vascular microcirculation.

The authors thank Prof. J. Cortijo for his help in defining the neutrophil isolation protocol, Dr. F. Rico for his assistance in the AFM technique, and M. Rodriguez for his technical assistance.

This work was supported in part by grants from Ministerio de Ciencia y Tecnologia (SAF2005-00110, SAF 2003-01334, and NAN2004-09348-C04-04) and Ministerio de Sanidad y Consumo (Red GIRA-G03/063, Red RESPIRA-C03/11, and FIS-PI040929).

## REFERENCES

1. Doerschuk, C. M. 2001. Mechanisms of leukocyte sequestration in inflamed lungs. *Microcirculation*. 8:71–88.
2. Vicente-Manzanares, M., and F. Sanchez-Madrid. 2004. Role of the cytoskeleton during leukocyte responses. *Nature Rev. Immunol.* 4: 110–122.
3. Doerschuk, C. M., N. Beyers, H. O. Coxson, B. Wiggs, and J. C. Hogg. 1993. Comparison of neutrophil and capillary diameters and their relation to neutrophil sequestration in the lung. *J. Appl. Physiol.* 74: 3040–3045.
4. Worthen, G. S., B. Schwab, E. L. Elson, and G. P. Downey. 1989. Mechanics of stimulated neutrophils—cell stiffening induces retention in capillaries. *Science*. 245:183–186.
5. Wojcikiewicz, E. P., X. H. Zhang, A. Chen, and V. T. Moy. 2003. Contributions of molecular binding events and cellular compliance to the modulation of leukocyte adhesion. *J. Cell Sci.* 116:2531–2539.
6. Spillmann, C. M., E. Lomakina, and R. E. Waugh. 2004. Neutrophil adhesive contact dependence on impingement force. *Biophys. J.* 87: 4237–4245.
7. Dong, C., and X. X. Lei. 2000. Biomechanics of cell rolling: shear flow, cell-surface adhesion, and cell deformability. *J. Biomech.* 33: 35–43.
8. Evans, E., and A. Yeung. 1989. Apparent viscosity and cortical tension of blood granulocytes determined by micropipet aspiration. *Biophys. J.* 56:151–160.
9. Needham, D., and R. M. Hochmuth. 1990. Rapid flow of passive neutrophils into a 4  $\mu\text{m}$ -M pipette and measurement of cytoplasmic viscosity. *J. Biomech. Eng.* 112:269–276.
10. Dong, C., R. Skalak, K. L. P. Sung, G. W. Schmid-schonbein, and S. Chien. 1988. Passive deformation analysis of human-leukocytes. *J. Biomech. Eng.* 110:27–36.
11. Sung, K. L. P., C. Dong, G. W. Schmid-Schonbein, S. Chien, and R. Skalak. 1988. Leukocyte relaxation properties. *Biophys. J.* 54:331–336.
12. Hochmuth, R. M., H. P. Tingbeall, B. B. Beaty, D. Needham, and R. Tran-Son-Tay. 1993. Viscosity of passive human neutrophils undergoing small deformations. *Biophys. J.* 64:1596–1601.
13. Skalak, R., D. Cheng, and Z. Cheng. 1990. Passive deformations and active motions of leukocytes. *J. Biomech. Eng.* 112:295–302.
14. Lipowsky, H. H., D. Riedel, and G. S. Shi. 1991. In vivo mechanical-properties of leukocytes during adhesion to venular endothelium. *Biorheology*. 28:53–64.
15. Yap, B., and R. D. Kamm. 2005. Cytoskeletal remodeling and cellular activation during deformation of neutrophils into narrow channels. *J. Appl. Physiol.* 99:2323–2330.
16. Fabry, B., G. N. Maksym, J. P. Butler, M. Glogauer, D. Navajas, N. A. Taback, E. J. Millet, and J. J. Fredberg. 2003. Time scale and other invariants of integrative mechanical behavior in living cells. *Phys. Rev. E.* 68:041914.

17. Sollich, P. 1998. Rheological constitutive equation for a model of soft glassy materials. *Phys. Rev. E*. 58:738–759.
18. Zhou, Y., C. M. Doerschuk, J. M. Anderson, and R. E. Marchant. 2004. Biomaterial surface-dependent neutrophil mobility. *J. Biomed. Mater. Res. A*. 69A:611–620.
19. Alcaraz, J., L. Buscemi, M. Grabulosa, X. Trepat, B. Fabry, R. Farre, and D. Navajas. 2003. Microrheology of human lung epithelial cells measured by atomic force microscopy. *Biophys. J.* 84:2071–2079.
20. Folkman, J., and A. Moscona. 1978. Role of cell shape in growth control. *Nature*. 273:345–349.
21. Russo-Carbolante, E. M. S., A. E. C. S. Azzolini, A. M. C. Polizello, and Y. M. Lucisano-Valim. 2002. Comparative study of four isolation procedures to obtain rat neutrophils. *Comp. Clin. Pathol.*. 441:71–76.
22. Rico, F., P. Roca-Cusachs, N. Gavara, R. Farre, M. Rotger, and D. Navajas. 2005. Probing mechanical properties of living cells by atomic force microscopy with blunted pyramidal cantilever tips. *Phys. Rev. E*. 72:021914.
23. Butt, H. J., and M. Jaschke. 1995. Calculation of thermal noise in atomic-force microscopy. *Nanotechnology*. 6:1–7.
24. Hutter, J. L., and J. Bechhoefer. 1993. Calibration of atomic-force microscope tips. *Rev. Sci. Instrum.* 64:1868–1873.
25. Alcaraz, J., L. Buscemi, M. Puig-de-Morales, J. Colchero, A. Baro, and D. Navajas. 2002. Correction of microrheological measurements of soft samples with atomic force microscopy for the hydrodynamic drag on the cantilever. *Langmuir*. 18:716–721.
26. Johnson, K. L. 1985. Contact Mechanics. Cambridge University Press, Cambridge.
27. Fung, Y. C. 1993. Biomechanics. Springer-Verlag, New York.
28. Lomakina, E. B., C. M. Spillmann, M. R. King, and R. E. Waugh. 2004. Rheological analysis and measurement of neutrophil indentation. *Biophys. J.* 87:4246–4258.
29. Fabry, B., G. N. Maksym, J. P. Butler, M. Glogauer, D. Navajas, and J. J. Fredberg. 2001. Scaling the microrheology of living cells. *Phys. Rev. Lett.* 87:148102.
30. Trepat, X., M. Grabulosa, F. Puig, G. N. Maksym, D. Navajas, and R. Farre. 2004. Viscoelasticity of human alveolar epithelial cells subjected to stretch. *Am. J. Physiol. Lung C*. 287:L1025–L1034.
31. Laudadio, R. E., E. J. Millet, B. Fabry, S. S. An, J. P. Butler, and J. J. Fredberg. 2005. Rat airway smooth muscle cell during actin modulation: rheology and glassy dynamics. *Am. J. Physiol. Cell Physiol.* 289: C1388–C1395.
32. Mahaffy, R. E., S. Park, E. Gerde, J. Kas, and C. K. Shih. 2004. Quantitative analysis of the viscoelastic properties of thin regions of fibroblasts using atomic force microscopy. *Biophys. J.* 86:1777–1793.
33. Rosenbluth, M. J., W. A. Lam, and D. A. Fletcher. 2006. Force microscopy of non-adherent cells: a comparison of leukemia cell deformability. *Biophys. J.* 90:2994–3003.
34. Kasas, S., and A. Ikai. 1995. A method for anchoring round shaped cells for atomic-force microscope imaging. *Biophys. J.* 68:1678–1680.
35. Zhelev, D. V., D. Needham, and R. M. Hochmuth. 1994. Role of the membrane cortex in neutrophil deformation in small pipets. *Biophys. J.* 67:696–705.
36. Mahaffy, R. E., C. K. Shih, F. C. MacKintosh, and J. Käs. 2000. Scanning probe-based frequency-dependent microrheology of polymer gels and biological cells. *Phys. Rev. Lett.* 85:880–883.
37. Stewart, M., and N. Hogg. 1996. Regulation of leukocyte integrin function: affinity vs avidity. *J. Cell. Biochem.* 61:554–561.
38. Lusciuskas, F. W., G. S. Kansas, H. Ding, P. Pizcueta, B. E. Schleiffenbaum, T. F. Tedder, and M. A. Gimbrone. 1994. Monocyte rolling, arrest and spreading on IL-4-activated vascular endothelium under flow is mediated via sequential action of L-selectin,  $\beta_1$ -integrins, and  $\beta_2$ -integrins. *J. Cell Biol.* 125:1417–1427.
39. Trepat, X., M. Grabulosa, L. Buscemi, F. Rico, R. Farre, and D. Navajas. 2005. Thrombin and histamine induce stiffening of alveolar epithelial cells. *J. Appl. Physiol.* 98:1567–1574.
40. Zhang, X. H., A. Chen, D. De Leon, H. Li, E. Noiri, V. T. Moy, and M. S. Goligorsky. 2004. Atomic force microscopy measurement of leukocyte-endothelial interaction. *Am. J. Physiol. Heart Circ. Physiol.* 286:H359–H367.
41. Sen, S., S. Subramanian, and D. E. Discher. 2005. Indentation and adhesive probing of a cell membrane with AFM. Theoretical model and experiments. *Biophys. J.* 89:3203–3213.
42. Wang, Q., E. T. Chiang, M. Lim, R. Rogers, P. A. Janmey, D. Shepro, and C. M. Doerschuk. 2001. Changes in the biomechanical properties of neutrophils and endothelial cells during adhesion. *Blood*. 97:660–668.
43. Yap, B., and R. D. Kamm. 2005. Mechanical deformation of neutrophils into narrow channels induces pseudopod projection and changes in biomechanical properties. *J. Appl. Physiol.* 98:1930–1939.
44. Yanai, M., J. P. Butler, T. Suzuki, H. Sasaki, and H. Higuchi. 2004. Regional rheological differences in locomoting neutrophils. *Am. J. Physiol. Cell Physiol.* 287:C603–C611.
45. Tsai, M. A., R. S. Frank, and R. E. Waugh. 1993. Passive mechanical behavior of human neutrophils: power-law fluid. *Biophys. J.* 65:2078–2088.
46. Lien, D. C., W. W. Wagner, R. L. Capen, C. Haslett, W. L. Hanson, S. E. Hofmeister, P. M. Henson, and G. S. Worthen. 1987. Physiological neutrophil sequestration in the lung—visual evidence for localization in capillaries. *J. Appl. Physiol.* 62:1236–1243.
47. Bathe, M., A. Shirai, C. M. Doerschuk, and R. D. Kamm. 2002. Neutrophil transit times through pulmonary capillaries: the effects of capillary geometry and fMLP-stimulation. *Biophys. J.* 83:1917–1933.
48. Tran-Son-Tay, R., T. F. Kirk, D. V. Zhelev, and R. M. Hochmuth. 1994. Numerical-simulation of the flow of highly viscous drops down a tapered tube. *J. Biomech. Eng.* 116:172–177.
49. Aoki, T., Y. Suzuki, K. Nishio, K. Suzuki, A. Miyata, Y. Iigou, H. Serizawa, H. Tsumura, Y. Ishimura, M. Suematsu, and K. Yamaguchi. 1997. Role of CD18-ICAM-1 in the entrapment of stimulated leukocytes in alveolar capillaries of perfused rat lungs. *Am. J. Physiol. Heart Circ. Physiol.* 273:H2361–H2371.